RSC Advances

PAPER

View Article Online
View Journal | View Issue

Cite this: *RSC Adv.*, 2015, **5**, 49235

Highly enterprising calcium zirconium phosphate [$CaZr_4(PO_4)_6$:Dy^{3+}, Ce^{3+}] phosphor for white light emission

Govind B. Nair and S. J. Dhoble*

A series of $CaZr_4(PO_4)_6$:Dy^{3+}, $CaZr_4(PO_4)_6$:Ce^{3+} and $CaZr_4(PO_4)_6$:Dy^{3+}, Ce^{3+} phosphors were prepared by the solid state reaction process. The phase formation was confirmed by X-ray powder diffraction (XRD) measurements. Morphological studies were performed using scanning electron microscopy. Raman spectra were studied to identify the scattering bands associated with the normal vibrational modes of the PO_4^{3-} tetrahedron. The photoluminescence properties of the phosphors were systematically investigated. With increasing Dy^{3+} concentration in $CaZr_4(PO_4)_6$:Dy^{3+} phosphor, the luminescence intensity first increases, reaches the maximum, and then decreases. A similar trend is followed by $CaZr_4(PO_4)_6$:Ce^{3+} phosphors, with increasing Ce^{3+} concentration. A successful attempt was made to initiate the energy transfer mechanism from Ce^{3+} to Dy^{3+} ions in the $CaZr_4(PO_4)_6$ host lattice. The CIE chromaticity coordinates of $CaZr_4(PO_4)_6$:Dy^{3+} phosphor exhibited emission near the white-light region and hence, it is a potential candidate for UV excited white-LEDs (WLEDs). $CaZr_4(PO_4)_6$:Dy^{3+}, Ce^{3+} phosphor has its CIE chromaticity coordinates in the white light region, near the standard illuminant D_{65}. Thermoluminescence (TL) studies on $CaZr_4(PO_4)_6$:Dy^{3+}, Ce^{3+} phosphor, which was performed to test its stability against low dose of gamma-ray exposure, are also documented.

Received 22nd April 2015
Accepted 28th May 2015

DOI: 10.1039/c5ra07306e

www.rsc.org/advances

1. Introduction

In the current scenario, the new generation LEDs are enjoying the upper hand over the conventionally used lighting sources due to their proficient, prolific and promising features such as enhanced luminous efficiency, reliability, higher energy efficiency and environmental friendliness.[1–3] Rigorous attempts are being made to improve the luminous efficiency, high chromatic stability and color rendering index of the LED light output. Usually, three distinct approaches can be used for obtaining white light emission from LEDs, and each of these methods suffer from several disadvantages.[4] One such way is to mix the light from several colored LEDs to create a spectral power distribution that appears white, or by preparing a perfect blend of red, green and blue phosphors which are then coated on the interior walls of an ultraviolet or near-ultraviolet LED. But the use of tricolour phosphor poses instability in the color temperature due to dissimilar degradation of different phosphors. Another way is to use blue LEDs to pump yellow phosphors, although problems like high color tolerance and low color rendering index may arise due to the lack of the red component. This approach was extensively used for many years, since it resulted in lower energy loss as compared to those in tricolour LED. To overcome these difficulties, a third type of approach was introduced in which single phase white light emitting phosphors are excited with UV-LEDs.[5]

Rare earth doped phosphors have gained immense attraction due to their high luminescence efficiency, color purity and long emission lifetimes. A number of rare earth doped phosphors were investigated to improve the qualities of the existing phosphors. Using the principle of energy transfer from the sensitizer to the activator, which has been introduced into a crystalline host matrix, it is possible to obtain white light from a single component phosphor. White light can also be obtained by adjusting the yellow to blue intensity ratio obtained by doping the host matrix with Dy^{3+} ion, as it has two intense emission bands in the blue (470–500 nm) and yellow region (560–600 nm) corresponding to the transitions $^4F_{9/2} \rightarrow {}^6H_{15/2}$ and $^4F_{9/2} \rightarrow {}^6H_{13/2}$ respectively.[6] The concentration of Dy^{3+} ions and the site symmetry of the host lattice around the Dy^{3+} ions strongly affect the intensity of these transitions and the relative yellow-to-blue (Y/B) intensity ratio gives the information concerned with the site symmetry around the Dy^{3+} ion in which it is situated.[7] The intensity of yellow transition is very sensitive and strongly influenced by the host environment while the intensity of blue transition is insensitive and hardly varies with the host environment.[8] The phenomenon of energy transfer from a rare earth ion acting as a sensitizer to the one acting as an activator is very well known to enhance the luminescence of rare earth ions.[9,10] One of the best candidates suitable for sensitizing is Ce^{3+} because of its unique electronic energy levels compared

Department of Physics, R.T.M. Nagpur University, Nagpur, India-440033. E-mail: sjdhoble@rediffmail.com

with other lanthanide ions.[9,11] Ce^{3+} gives a strong broad emission due to the allowed 4f–5d electric dipole transition with a very high absorption cross section in an order of 10^{-18} cm^2. The host dependent nature of the absorption and emission bands of Ce^{3+} plays a crucial role in promoting efficient energy transfer from Ce^{3+} ions to the acceptor rare earths.

Several types of phosphors such as oxides,[12,13] sulphides,[14] orthosilicates,[15] nitrides,[16,17] aluminates,[18] *etc.* are used in LEDs. However, it is difficult to couple oxide-based phosphors with blue LED due to their low absorption in the visible light spectrum. On the other hand, the luminescence characteristics of sulphide based phosphors degrade due to their sensitivity to moisture and thermal instability.[16] Moreover, some nitride phosphors demand sophisticated pre-requisites and critical preparation conditions for synthesis[17,19] and are vulnerable to lose efficiency over time in pc-LED packages.[20] Excellent luminescence properties of orthophosphates have given them good consideration to act as a host matrix for luminescent materials. They exhibit large band gap and high absorption of PO_4^{3-} in VUV region, moderate phonon energy, high chemical stability, exceptional optical damage threshold and low sintering temperature. $CaZr_4(PO_4)_6$ belongs to a new family of phosphors with low thermal expansion, flexible structure, low thermal conductivity, fast ionic conductivity and high stability against leaching reactions.[21,22] Luminescent properties of $CaZr_4(PO_4)_6$ phosphor doped by Eu^{3+} and Dy^{3+} has been reported earlier.[6,23,24] However, no studies have been reported on the luminescent properties of Ce^{3+} activated $CaZr_4(PO_4)_6$ phosphor and the energy transfer from Ce^{3+} to Dy^3 ions, till date.

The current work signifies the energy transfer phenomenon from Ce^{3+} to Dy^{3+} ions in the $CaZr_4(PO_4)_6$ host matrix. The host matrix was individually doped with Ce^{3+} and Dy^{3+} ions to inspect the consistency between the emission band of Ce^{3+} ions and the excitation band of Dy^{3+} ions.

2. Experimental

2.1 Synthesis

The powder samples of the phosphors $Ca_{1-x}Zr_4(PO_4)_6{:}xDy^{3+}$, $Ca_{1-x}Zr_4(PO_4)_6{:}xCe^{3+}$ and $Ca_{0.9}Zr_4(PO_4)_6{:}0.05Dy^{3+}$, 0.05Ce ($x = 0.02, 0.03, 0.04, 0.05, 0.06$) were prepared by the solid state reaction method in ambient air atmosphere. The precursors were $CaCO_3$ (99% pure) procured from Lobachemie, ZrO_2 (99% pure) procured from Sisco Research Laboratories, NH_6PO_4 (99% pure) procured from Sisco Research Laboratories and, Ce_2O_3 and Dy_2O_3 (99.9% pure) procured from Lobachemie. All the precursors were of analytical grade and were mixed in stoichiometric proportion. The starting materials were effectively crushed into fine powder in a porcelain mortar using pestle. They were emptied into porcelain crucibles and kept for heating for 2 hours at 450 °C. The samples emerged out from the crucibles in the form of solid foam. After complete cooling, the samples were again crushed to fine powder. The intermittent crushing, between the consecutive heat treatments, helps to break the possibly developed grain boundaries and thereby enhances the diffusion amongst the atoms. The resulting samples were further annealed at 800 °C for 14 hours and subsequently cooled to room temperature.

2.2 Characterization

The X-ray diffraction (XRD) pattern of $CaZr_4(PO_4)_6$ phosphor was collected in the 2θ range 10° to 100° with the step size of 0.0170° using a PANalytical X'pert PRO X-ray diffractometer with Cu-Kα radiation ($\lambda = 1.54060$ Å) operating at 40 kV and 25 mA at 25 °C. The morphological studies were carried out by the JEOL JSM-6380 scanning electron microscope (SEM). A Raman spectrum of the as-prepared $Ca_{1-x}Zr_4(PO_4)_6{:}0.05Dy^{3+}$, 0.05Ce phosphor was obtained. The photoluminescence excitation and emission spectra were measured at room temperature using RF-5301PC Shimadzu spectrofluorophotometer with a slit width of 1.5 nm and a 150 W xenon lamp as the excitation source. The CIE chromaticity coordinates were determined using Radiant Imaging color calculator software. For the thermoluminescence (TL) study, the $Ca_{1-x}Zr_4(PO_4)_6{:}0.05Dy^{3+}$, 0.05Ce phosphor was irradiated with 2.6 Gy of γ-rays from a ^{60}Co source for a duration of 30 s at room temperature. After the desired exposure, TL glow curves were recorded with the help of Nucleonix 1009I TL reader, at a heating rate of 5 °C s^{-1}. The TL readings were recorded for 5 mg of phosphor in the temperature range 45–400 °C in an open atmosphere.

3. Results and discussion

3.1 X-ray diffraction and crystal structure analysis

Fig. 1 represents the XRD pattern of $CaZr_4(PO_4)_6$ host lattice synthesized by solid state reaction method. The XRD pattern matched perfectly with the standard data available in JCPDS card no. 33-0321. No impurity phases or peaks were observed in the pattern giving a direct indication of a homogeneous phase formation. Some lower intensity peaks may have got lost in the background noise, which may be attributed to the instrumental error.

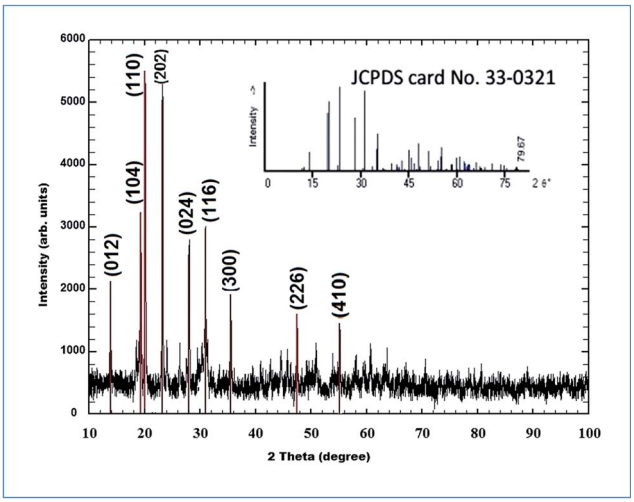

Fig. 1 X-ray diffraction pattern of the $CaZr_4(PO_4)_6$ host lattice.

$CaZr_4(PO_4)_6$ is classified as a rhombohedral structure with space group $R\bar{3}c$ (no. 161) and the lattice parameters are given as: $a = b = 8.785$ Å, $c = 22.862$ Å, $\alpha = \beta = 90°$, $\gamma = 120°$. The ionic radii of Dy^{3+} and Ce^{3+} are most compatible with the ionic radii of Ca^{2+} ions. Hence, doping of these rare earth ions are confirmed to occur at Ca^{2+} lattice sites.[6,23] Since the concentration of the dopants is negligible, no distortion will be observed in the crystal structure of the host lattice. As a result, the XRD pattern will also show consistency with increasing dopant concentration. This has been experimentally proved and reported previously by several researchers.[6,23] Using the Visualization for Electronic and Structural Analysis (VESTA) program, version 3.1.8 for Windows, a unit cell was modelled as shown in Fig. 2.[25] Zr atoms are displaced from the centre of the octahedron due to the Ca^{2+}–Zr^{4+} repulsions. As a result, the Zr–O(2) distance, neighbouring the Ca(1) site, is slightly greater than the Zr–O(1) distance. The approximate variation of the O–Zr–O angle ranges from 77° to 180°, whereas that of O–P–O ranges from 106° to 112°.[26]

3.2 Scanning electron microscopy

SEM micrographs of $CaZr_4(PO_4)_6$ phosphor synthesized by solid state reaction method are shown in Fig. 3. The particles possess foam-like morphology and several pores could be observed on the surface which are formed by the residual gases that has escaped during the synthesis. The crystallites are highly agglomerated and suggest formation of spherical agglomerated particles. Doping does not have any considerable effect on the surface morphology in these micrographs. The size of the as-prepared phosphors ranged from 0.8 μm to 1.26 μm, and this is suitable for solid state lighting.

3.3 Raman Spectroscopy

The Raman spectrum of the as-prepared $Ca_{0.95}Zr_4(PO_4)_6{:}Dy_{0.05}$ phosphor is shown in the Fig. 4. The basic vibration modes from $(PO_4)^{3-}$ free ions have four modes, *viz.*, ν_1 of P–O symmetric stretching vibration, ν_2 of O–P–O symmetric bending vibration, ν_3 of P–O asymmetric stretching vibration and ν_4 of O–P–O asymmetric bending vibration in the $(PO_4)^{3-}$ tetrahedron. There may be some changes in the $(PO_4)^{3-}$ vibration in the crystal structure, due to the disorder in the local point symmetry and anion O^{2-}.[27] A very weak band positioned at 970 cm^{-1} is assigned to the $\nu_1(PO_4)^{3-}$ symmetric stretching vibration. A strong band at 484 cm^{-1} and two moderately strong bands at 424 cm^{-1} and 437 cm^{-1} are assigned to $\nu_2(PO_4)^{3-}$ symmetric bending vibrations. A strong band at 1029 cm^{-1} and two moderately strong bands at 1065 cm^{-1} and 1087 cm^{-1} are assigned to $\nu_3(PO_4)^{3-}$ asymmetric stretching vibrations, whereas three weak bands at 561 cm^{-1}, 574 cm^{-1} and 641 cm^{-1} are assigned to $\nu_4(PO_4)^{3-}$ asymmetric bending vibrations.

3.4 Photoluminescence study

3.4.1 Photoluminescence of $CaZr_4(PO_4)_6{:}xDy^{3+}$. Fig. 5 depicts the PL excitation spectra of $CaZr_4(PO_4)_6{:}xDy^{3+}$ ($x = 0.02$, 0.03, 0.04, 0.05, 0.06) phosphors monitored at 576 nm. The sharp excitation peaks from 300 nm to 500 nm can be attributed

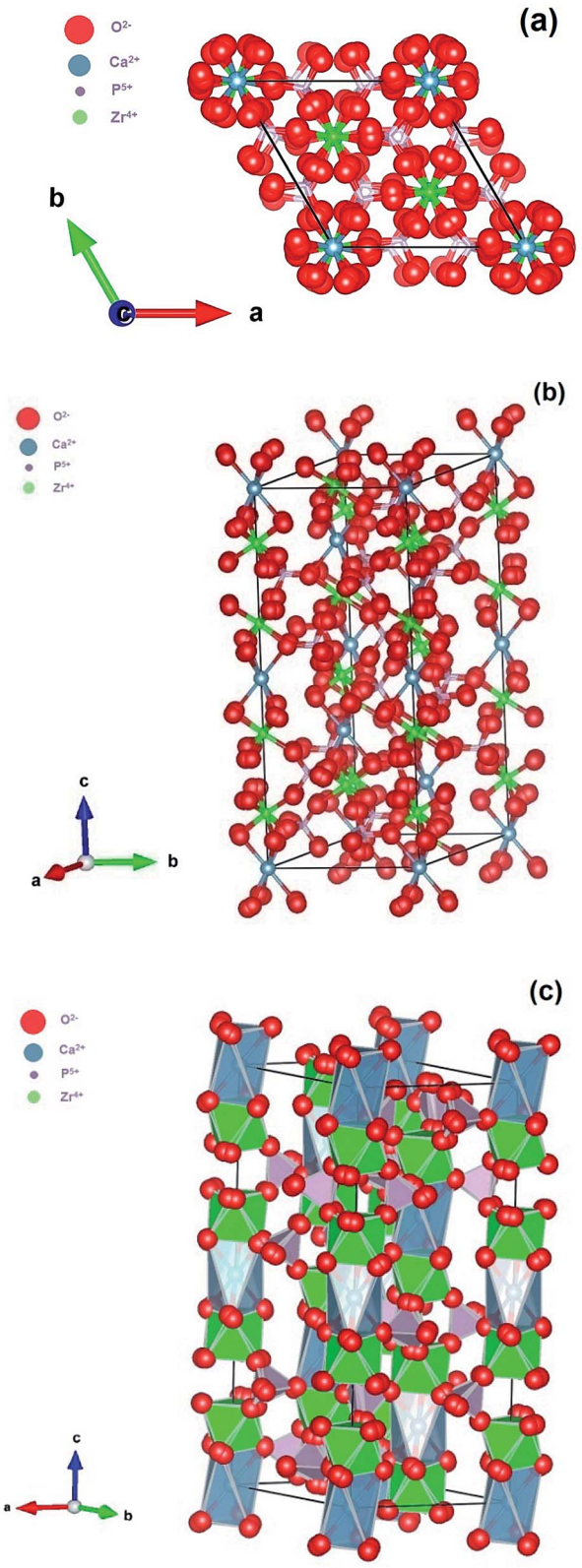

Fig. 2 Unit cell representation of crystal structure of $CaZr_4(PO_4)_6$. (a) Structure viewed along *c*-axis, (b) ball and stick model representation, and (c) polyhedral representation of $CaZr_4(PO_4)_6$.[26]

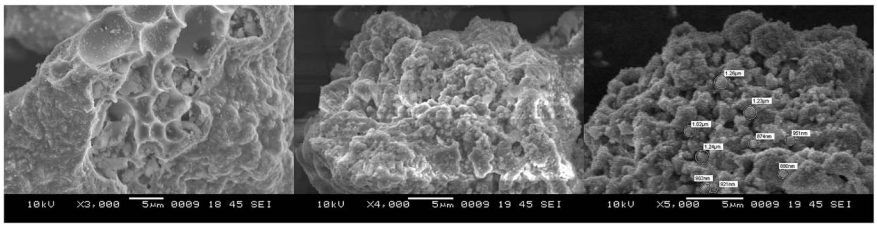

Fig. 3 SEM micrographs of $CaZr_4(PO_4)_6$ phosphor synthesized by solid state reaction method.

to the intra-4f forbidden transitions from the ground state $^6H_{15/2}$ to higher energy levels of Dy^{3+}. It consists of a series of sharp peaks located at 326 nm, 351 nm, 365 nm, 391 nm, 426 nm, 455 nm and 477 nm, corresponding to the transitions from $^6H_{15/2}$ to $^4M_{17/2}$, $^6P_{7/2}$, $^6P_{5/2}$, $^4F_{7/2}$, $^4G_{11/2}$, $^4I_{15/2}$ and $^4F_{9/2}$ respectively. Hence, it is quite evident that the phosphor can be excited by ultraviolet light, near ultraviolet light (NUV) as well as blue light. Among these, the most intense transition was observed at 351 nm indicating their potential to be used in NUV white LEDs. Another intense peak is evident at 455 nm, and this marks its significance to be used in LEDs with blue light excitation. However, although f → f transitions are, in principle, forbidden by the Laporte parity rule, most of the transitions in $(RE)^{3+}$ ions occur at the electric dipole (ED) order.[28] This is an ED allowance due to the admixture of the $4f^n$ states with opposite parity excited states $4f^{n-1}5d$, as a result of the lack of inversion symmetry (ED forced transitions).

The emission spectra of $CaZr_4(PO_4)_6$:xDy^{3+} phosphors excited at 351 nm are shown in the Fig. 6. Two dominating emissions are apparent around 483 nm and 576 nm corresponding to the $^4F_{9/2} \rightarrow {}^6H_{15/2}$ and $^4F_{9/2} \rightarrow {}^6H_{13/2}$ transitions respectively. The $^4F_{9/2} \rightarrow {}^6H_{15/2}$ transition can be stated as a magnetic dipole transition, whereas the $^4F_{9/2} \rightarrow {}^6H_{13/2}$ transition can be attributed to a forced electric dipole transition. The former case is allowed when the Dy^{3+} ions occupies the local sites with inversion centre symmetry, while the latter case is allowed only in the case when the Dy^{3+} ions occupies the local sites with non-inversion centre symmetry.[29,30] Thus, the stronger

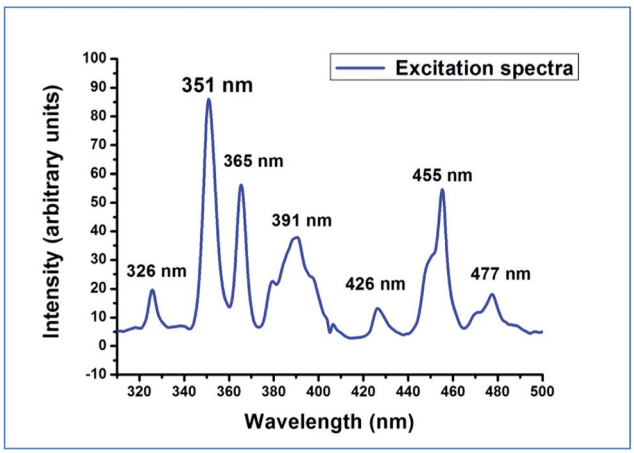

Fig. 5 PL excitation spectrum of $CaZr_4(PO_4)_6$:xDy^{3+} phosphor.

blue emission indicates that the Dy^{3+} ions are in a site with inversion symmetry. A series of $Ca_{1-x}Zr_4(PO_4)_6$:xDy^{3+} ($x = 0.02$, 0.03, 0.04, 0.05, 0.06) phosphors were synthesized to investigate the influence of different Dy^{3+} doping concentrations. Fig. 6 shows the variation in the emission intensities for different concentrations of Dy^{3+} ions. The emission spectra depict a similar profile for all the concentrations. However, the peak intensity is found to increase when the dopant concentration varies from $x = 0.02$ to 0.05. The optimum peak intensity of emission is obvious at $x = 0.05$ and a further increase in Dy^{3+} concentration subsequently decreases the peak intensity. Here,

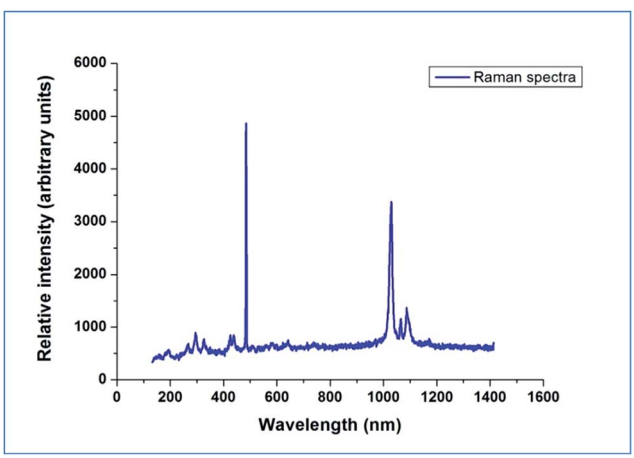

Fig. 4 Raman spectrum of $CaZr_4(PO_4)_6$ phosphor.

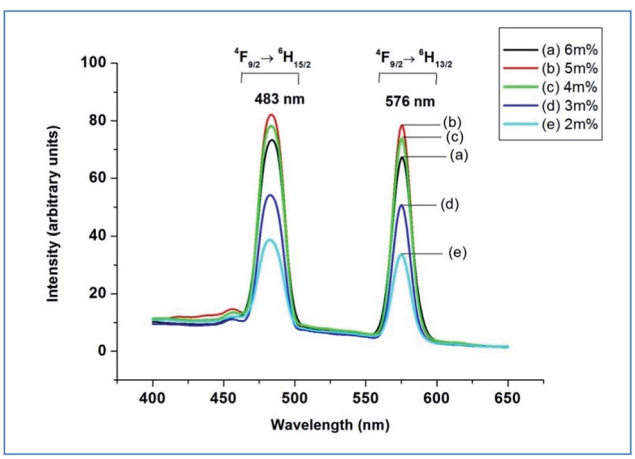

Fig. 6 PL emission spectra of $CaZr_4(PO_4)_6$:xDy^{3+} phosphor.

$x = 0.05$ is considered as the critical concentration. Fig. 7 portrays the variation in the peak intensity of $^4F_{9/2} \rightarrow {}^6H_{15/2}$ and $^4F_{9/2} \rightarrow {}^6H_{13/2}$ transitions with the varying concentration of Dy^{3+} ions in the $CaZr_4(PO_4)_6$ host lattice. Thus, the intensity of emission increases with increasing Dy^{3+} concentration and a slight excess beyond the critical concentration will result in concentration quenching. The concentration quenching occurs due to the promotion of non-radiative energy transfers between Dy^{3+} ions. This is a direct consequence of the increasing concentration of Dy^{3+} ions, since increasing concentration is responsible for decreasing the distance between the Dy^{3+} ions. Fig. 9 gives the energy level scheme to explain the emission process in $Ca_{1-x}Zr_4(PO_4)_6{:}xDy^{3+}$ phosphors.[31]

The quenching of luminescence intensity is primarily caused by the non-radiative energy transfer among Dy^{3+} ions, which occurs due to an exchange interaction, radiation reabsorption, or a multipole–multipole interaction, and the quenching phenomenon elucidates its dependency on the critical energy transfer distance R_c. R_c is the shortest average distance between the nearest activator Dy^{3+} ions at a critical concentration. The value of the critical distance, R_c can be evaluated using the Blasse formula,[32]

$$R_c = 2\left(\frac{3V}{4\pi X_c N}\right)^{\frac{1}{3}}$$

where V is the volume of the unit cell, X_c is the critical concentration of Dy^{3+} ions, and N is the number of available sites for the dopant in the unit cell. For the $CaZr_4(PO_4)_6$ host, $V = 1527.32$ Å^3, $X_c = 0.05$ and $N = 3$, consequently, the value of R_c is calculated to be 26.89 Å. However, when the critical distance among the Dy^{3+} ions is greater than 5 Å, the exchange interaction becomes ineffective, and a multipolar interaction becomes significant.[33] The strength of the multipolar interaction can be determined from the change in the emission intensity from the emitting level which has the multipolar interaction.[23,34] When the concentration of the dopant is sufficiently high, the luminescence intensity I and the dopant concentration x are related by the equation,

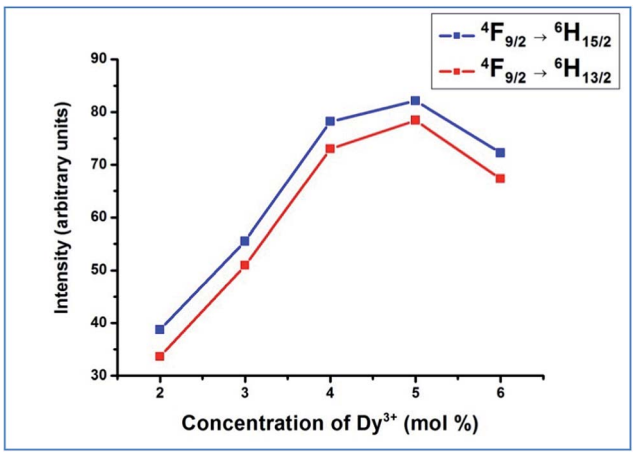

Fig. 7 Relation between PL intensity of $^4F_{9/2} \rightarrow {}^6H_{15/2}$ and $^4F_{9/2} \rightarrow {}^6H_{13/2}$ transitions with concentration of Dy^{3+}.

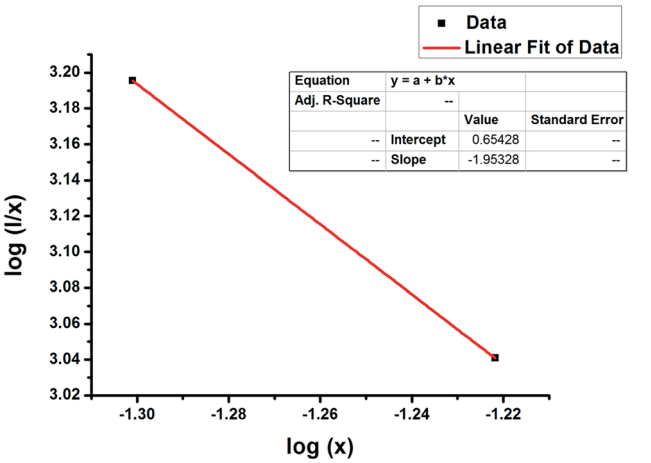

Fig. 8 The linear plot of $\log(I/x)$ *versus* $\log(x)$ plot for $CaZr_4(PO_4)_6{:}x Dy^{3+}$ phosphors.

$$\frac{I}{x} = k\left[1 + \beta x^{\frac{\theta}{3}}\right]^{-1}$$

This equation can be approximated as,

$$\log\frac{I}{x} = c - \frac{\theta}{3}\log x$$

where, k, β and c are constants for the same excitation condition for a given host matrix. θ is the index of electric multipole and it corresponds to electric dipole–dipole (d–d), electric dipole–electric quadrupole (d–q) and electric quadrupole–electric quadrupole (q–q) interactions, respectively, when its value is 6, 8 and 10. Fig. 8 illustrates the correlation between $\log(I/x)$ and $\log(x)$ for $CaZr_4(PO_4)_6{:}xDy^{3+}$ ($x \geq 0.05$) phosphor, on the basis of its emission spectra obtained at 351 nm. Since the interaction of ions after concentration quenching is more complicated,[23] only two points ($x = 0.05$ and 0.06) have been selected for plotting. Upon analysis of this plot, the data was found to fit a straight line with a slope, $\left(-\frac{\theta}{3}\right) \approx -1.9533$. Hence, the value of θ is 5.8599, which is approximately equal to 6. This gives an obvious

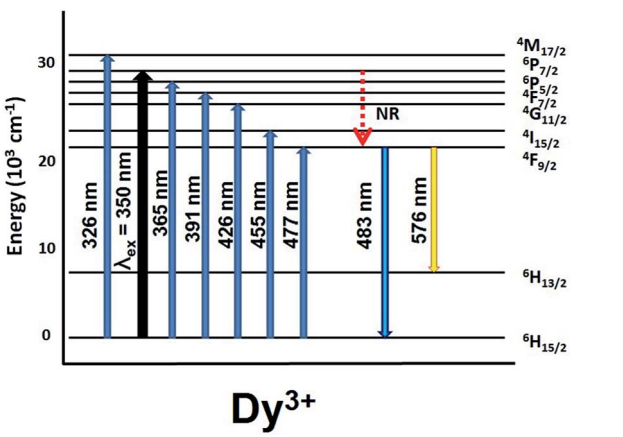

Fig. 9 Energy level scheme of Dy^{3+} in $CaZr_4(PO_4)_6$.

indication that the electric dipole–dipole interaction mechanism is the dominant mechanism responsible for the concentration quenching of Dy^{3+} emission in $CaZr_4(PO_4)_6$:xDy^{3+} phosphors.

3.4.2 Photoluminescence of $CaZr_4(PO_4)_6$:xCe^{3+}. Since Ce^{3+} has only one outer electron and only two spin-orbital splitting 4f states, *viz.* $^2F_{5/2}$ and $^2F_{7/2}$, it has a very simple excited state energy structure as compared to other rare earth ions. In Fig. 10, the PL excitation spectrum of Ce^{3+} ions in the $CaZr_4(PO_4)_6$ host lattice, monitored at 350 nm, exhibits broad band emission with peaks at 256 nm, 276 nm and 314 nm, which correspond to transitions from the ground state to the different crystal field splitting levels of the $5d^1$ states for Ce^{3+}. The most prominent peak is identified at 276 nm.

Fig. 11 displays the emission spectra of a series of $CaZr_4(PO_4)_6$:xCe^{3+} phosphors with different concentrations of doping, excited at 276 nm. The phosphors exhibit broad band emission extending from 310 to 390 nm with a maximum at about 338 nm when excited by 276 nm UV light and does not change with varying excitation wavelength except for the differences in intensity. It is a known reality that the Ce^{3+} emission should be composed of a double band due to the splitting of its 4f ground state, and the energy difference of this splitting between $^2F_{7/2}$ and $^2F_{5/2}$ of Ce^{3+} is about 2000 cm^{-1}. However, the doublet bands of the emission spectrum cannot be distinguished directly and hence, it is resolved into two well-separated Gaussian components with peak centres at 30 581 cm^{-1} (327 nm) and 28 818 cm^{-1} (347 nm) on the energy scale, as shown in the Fig. 12. The energy difference between these two bands is 1763 cm^{-1} and this is very close to the theoretical energy difference between the $^2F_{7/2}$ and $^2F_{5/2}$ levels, which is about 2000 cm^{-1}.[35] This implies that there is only one type of Ce^{3+} luminescence site in the $CaZr_4(PO_4)_6$ host lattice,[36] and Ca site is found to be the most appropriate crystallographic site available for Ce^{3+} doping. The Stokes shift, which is found to be approximately 6646 cm^{-1}, is in the normally reported value for Ce^{3+} doped phosphors in the range 3200–7200 cm^{-1}.[37] There is a slight shift in the position of peak intensity to the longer wavelength side, *i.e.* low energy, with increasing Ce^{3+}-doping concentration.

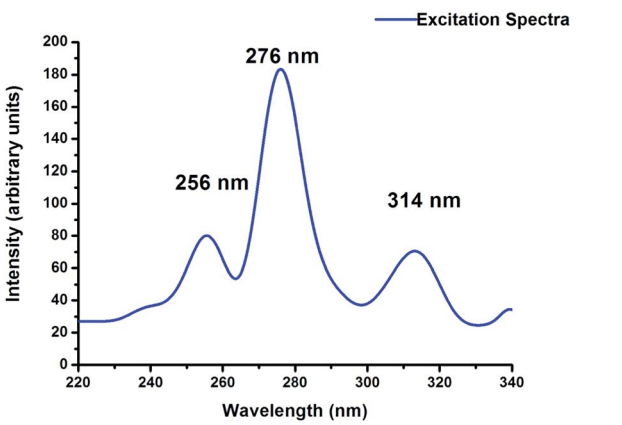

Fig. 10 PL excitation spectrum of $CaZr_4(PO_4)_6$:xCe^{3+} phosphor.

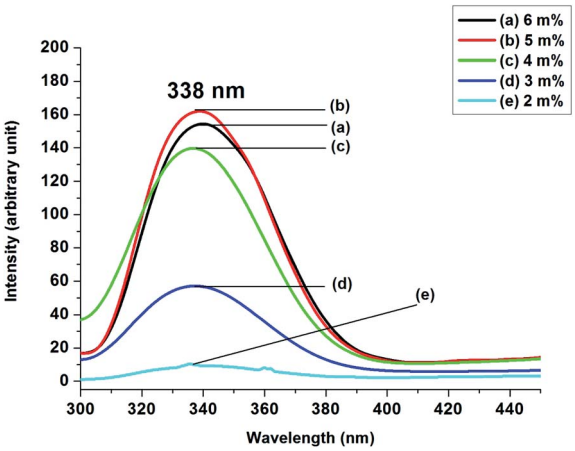

Fig. 11 PL emission spectra of $CaZr_4(PO_4)_6$:xCe^{3+} phosphor.

Fig. 13 shows the variation of PL intensity of $CaZr_4(PO_4)_6$:xCe^{3+} phosphors with Ce^{3+}-doping concentration. It can be observed that the emission intensity of the Ce^{3+} ions initially increases with increasing doping concentration, until it reaches a maximum at $x = 0.05$. Thereafter, the intensity decreases with a further increase in concentration due to the concentration quenching effect. The critical energy transfer distance R_c can be calculated between Ce^{3+} ions using the same procedure that was previously followed in case of Dy^{3+} ions, and it is found that the same value of R_c is retained in both the cases. Fig. 14 shows the fit of $\log(I/x)$ *versus* $\log(x)$ in $CaZr_4(PO_4)_6$:xCe^{3+} phosphors, with a slope of -1.00. The value of θ is calculated to be 3. According to results published by Van Uitert, $\theta = 3$ corresponds to the energy transfer among the nearest-neighbor ions.[38] This confirms that the concentration quenching mechanism of Ce^{3+} emission was dominated by the energy transfer among the nearest-neighbour ions.

3.4.3 Energy transfer. Ce^{3+} ion is a well-known sensitizer for trivalent rare earth ion luminescence and their sensitizing effects are strongly dependent on the host matrix, wherein these ions get introduced.[39] For efficient energy transfer from the

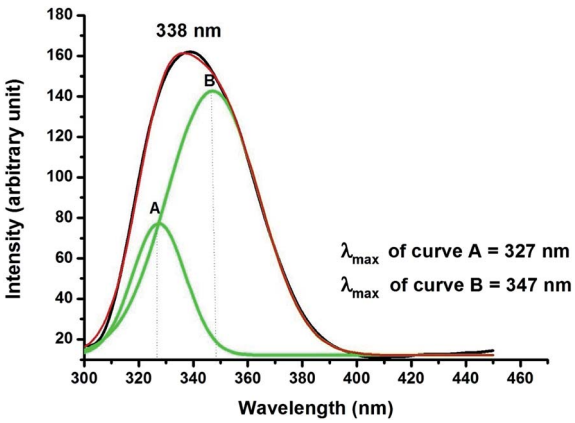

Fig. 12 The PL spectrum of $CaZr_4(PO_4)_6$:Ce^{3+} with the emission peak at 338 nm fitted by Gaussian functions (λ_{exc} = 276 nm).

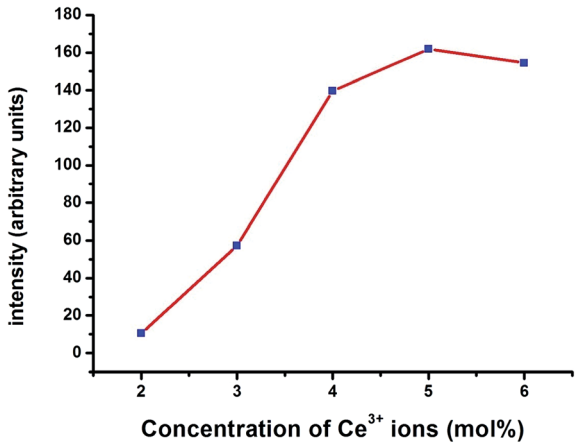

Fig. 13 Variation of PL intensity of $CaZr_4(PO_4)_6$:Ce^{3+} phosphors with doping concentration of Ce^{3+} ions.

sensitizer to the activator ion, the most significant requirement is that there should be a spectral overlap between the emission spectrum of the sensitizer and the absorption spectrum of the activator.[4] Here, Dy^{3+} acts as an activator and Ce^{3+} as a sensitizer. Comparing the PL excitation spectrum of $CaZr_4(PO_4)_6$:$0.05Dy^{3+}$ with the PL emission spectrum of $CaZr_4(PO_4)_6$:$0.05Ce^{3+}$, the emission band of Ce^{3+} in the range 310–390 nm overlaps with the excitation peaks of Dy^{3+} located within the range 320–390 nm.

Fig. 15 gives a schematic representation of the energy transfer mechanism from Ce^{3+} to Dy^{3+} ion pair in the $CaZr_4(PO_4)_6$ host matrix. Fig. 16 shows the PL excitation spectrum of $CaZr_4(PO_4)_6$:$0.05Dy^{3+}$, $0.05Ce^{3+}$ phosphor monitored at 576 nm, which is the prominent emission of Dy^{3+}. The 4f → 5d transition of Ce^{3+} is clearly visible in the excitation spectrum and this suggests the occurrence of energy transfer from Ce^{3+} to Dy^{3+} ions. This inference is in good sync with the earlier made expectation of possible energy transfer from Ce^{3+} to Dy^{3+} ions considering the spectral overlap between the emission transitions of Ce^{3+} and the absorption transitions of Dy^{3+} ions.

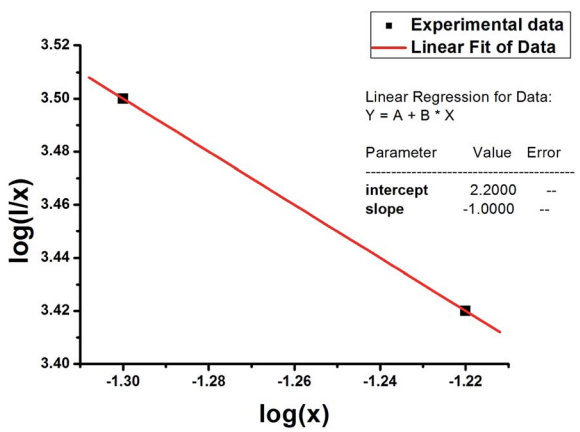

Fig. 14 The linear plot of $\log(I/x)$ *versus* $\log(x)$ plot for $CaZr_4(PO_4)_6$:xCe^{3+} phosphors.

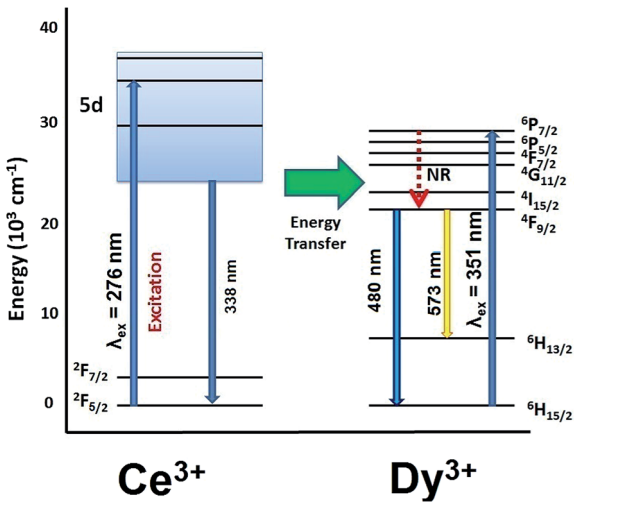

Fig. 15 Illustration of the energy transfer mode for Ce^{3+} to Dy^{3+} ion pair in the $CaZr_4(PO_4)_6$ host matrix.

Fig. 17 shows the emission spectrum of $CaZr_4(PO_4)_6$:$0.05Dy^{3+}$, $0.05Ce^{3+}$ phosphor, excited at 276 nm UV light. The Dy^{3+} emission is enforced by the introduction of Ce^{3+} and this is attributed to the energy transfer phenomena from the Ce^{3+} ion to the Dy^{3+} ion in the $CaZr_4(PO_4)_6$ host material. The emission spectrum of cerium and dysprosium codoped $CaZr_4(PO_4)_6$ phosphor exhibits the $^4F_{9/2} \rightarrow {}^6H_{15/2}$ and $^4F_{9/2} \rightarrow {}^6H_{13/2}$ emissions of Dy^{3+}, in addition to the Ce^{3+} emission band. When excited with 276 nm UV wavelength, the $CaZr_4(PO_4)_6$:Dy^{3+}, Ce^{3+} phosphor shows three emission peaks at around 338 nm, 480 nm and 573 nm. Upon 276 nm UV excitation, a part of the excited Ce^{3+} ions radiate to its ground state $^2F_{5/2}$ through 338 nm emission and the rest of the Ce^{3+} ions transfer their energy to Dy^{3+} ions. The Dy^{3+} ions get excited by absorbing this energy, but decays very quickly to the metastable state $^4F_{9/2}$ through non-radiative energy transfer and thereafter, results in radiative emissions through $^4F_{9/2} \rightarrow {}^6H_{15/2}$ and $^4F_{9/2} \rightarrow {}^6H_{13/2}$.

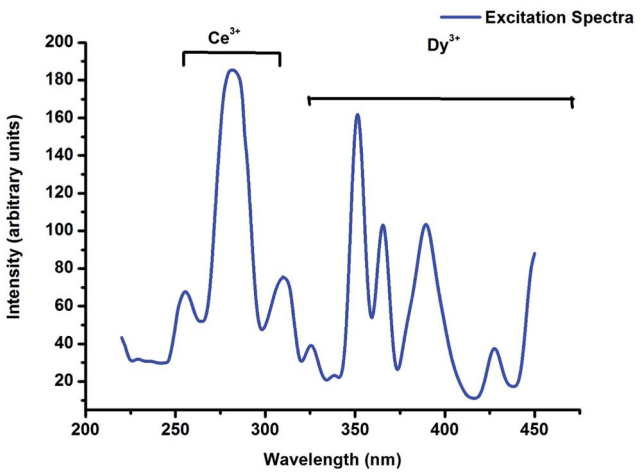

Fig. 16 PL excitation spectra of $CaZr_4(PO_4)_6$:$0.05Dy^{3+}$, $0.05Ce^{3+}$ phosphor.

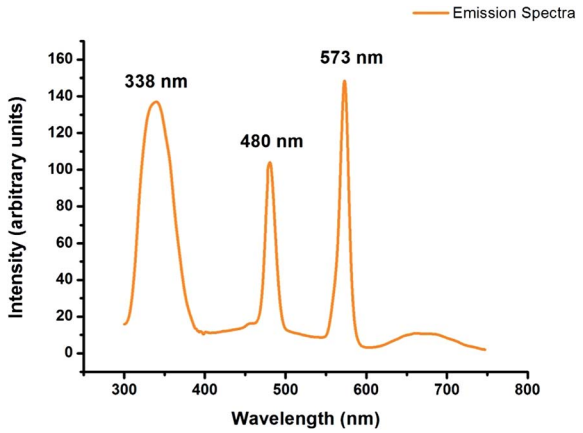

Fig. 17 PL emission spectra of $CaZr_4(PO_4)_6$:0.05Dy^{3+}, 0.05Ce^{3+} phosphor.

It is interesting to note that the intensity ratio of yellow to blue (Y/B) emissions of Dy^{3+} increases substantially when the Ce^{3+} co-doped phosphor are excited at 276 nm. This is in contrast to the Dy-doped phosphor, which showed the Y/B ratio less than unity. This gives the indication that Dy^{3+} ions occupy the lower symmetry local sites with non-inversion centre in $CaZr_4(PO_4)_6$:Dy^{3+}, Ce^{3+} phosphor. The sensitizing action of Ce^{3+} ions is responsible for the changes in local sites from higher to lower symmetry, under 273 nm UV excitation.[8]

Fig. 18 shows the PL emission spectra of $CaZr_4(PO_4)_6$:0.05Dy^{3+}, 0.05Ce^{3+}, $CaZr_4(PO_4)_6$:xDy^{3+} and $CaZr_4(PO_4)_6$:x5Ce^{3+} phosphors. It is evident that the peak intensity of Ce^{3+} in codoped phosphor is slightly less than that in case of Ce^{3+} doped phosphor. However, the Dy^{3+} emissions in the codoped phosphor are found to be slightly better than that in case of Dy^{3+} doped phosphor. The blue emission enhanced by 1.4 times whereas the yellow emission enhanced by 1.9 times after introducing the phosphor with the co-dopant Ce^{3+} ions.

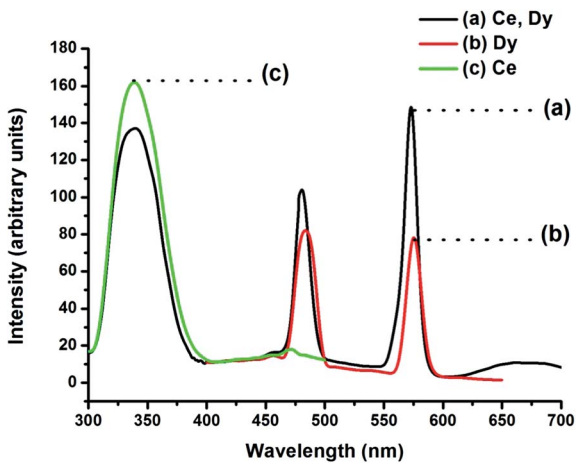

Fig. 18 PL emission spectra of (a) $CaZr_4(PO_4)_6$:0.05Dy^{3+}, 0.05Ce^{3+} at λ_{exc} = 276 nm, (b) $CaZr_4(PO_4)_6$:xDy^{3+} at λ_{exc} = 351 nm and (c) $CaZr_4(PO_4)_6$:x5Ce^{3+} at λ_{exc} = 276 nm phosphors.

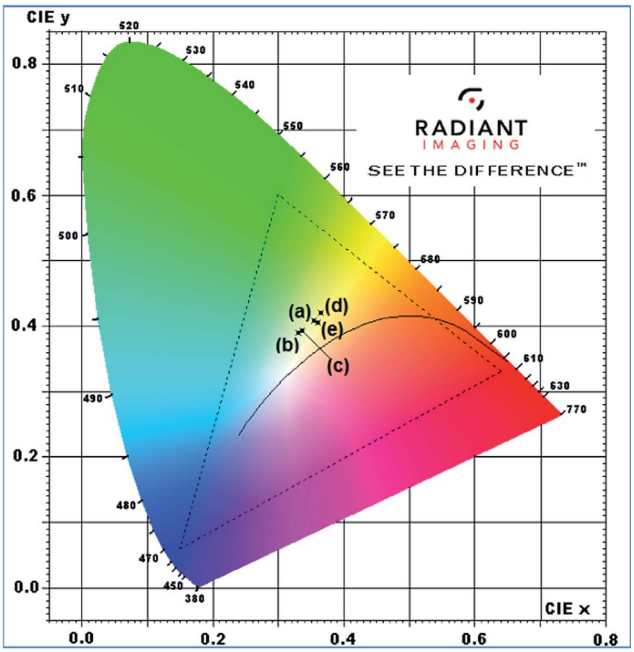

Fig. 19 CIE chromaticity coordinates of $CaZr_4(PO_4)_6$:xDy^{3+} phosphors.

3.5 Photometric characterization

The Commission Internationale de l'Eclairage (CIE) parameters such as color coordinates and correlated color temperature (CCT) were calculated in order to know the photometric characteristics of the as-prepared phosphors. CIE 1931 *x*–*y* chromaticity diagram of $CaZr_4(PO_4)_6$:Dy^{3+} (x = 0.02, 0.03, 0.04, 0.05,and 0.06) phosphors are presented in Fig. 19. Fig. 20 represents the CIE 1931 *x*–*y* chromaticity diagram of $CaZr_4(PO_4)_6$:Dy^{3+}, Ce^{3+} phosphor. The parameters were calculated by the spectrophotometric method using the spectral energy distribution of chromaticity diagram and are summarized in Table 1. The Y/B intensity ratio for 2%, 3%, 4%, 5% and 6% concentration of Dy^{3+} in the phosphors are 0.8686, 0.9357, 0.9358, 0.9512 and 0.9158 respectively. The CIE chromaticity coordinates for these phosphors are located in the near-white region and they hardly show any change with increasing concentration. An earlier report claimed this phosphor to show emission in the warm-white light region,[23] but this was later contradicted by another report which suggested bluish-white light emission from this phosphor.[6] In the present case, the correlated color temperatures (CCT) suggest the emission to be cool-white or bluish-white and therefore, the phosphor has potential applications in UV-based white LEDs, especially for indoor illumination. The Y/B intensity ratio of $CaZr_4(PO_4)_6$:0.05Dy^{3+}, 0.05Ce^{3+} phosphor is 1.432. However, the CIE chromaticity coordinate for this phosphor is found to be (0.3114, 0.3501), which is located in the white light region. This position is very near to that of the D_{65} illuminant, for which the CIE coordinates are (0.3127, 0.3290).[40–42] Hence, this phosphor can be suggested for application as a noon daylight simulator since its white light emission has comparable CIE

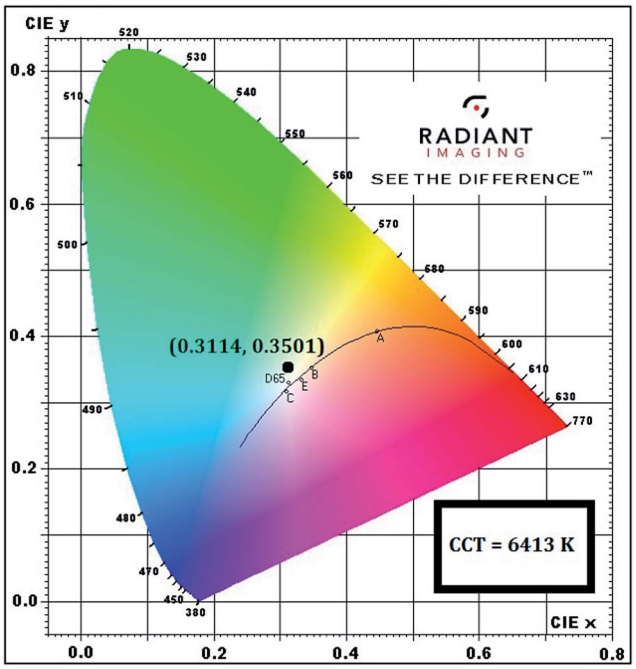

Fig. 20 CIE chromaticity coordinates of $CaZr_4(PO_4)_6$:0.05Dy^{3+}, 0.05Ce^{3+} phosphor.

chromaticity coordinates and CCT with that of the noon daylight.

3.6 Thermoluminescence study

Generally, thermoluminescence studies are performed on a material with a view to use it for radiation dosimetric applications.[43] However, in the present work, TL studies were performed to test the quality of the phosphor. The TL glow peak of $CaZr_4(PO_4)_6$:Dy^{3+}, Ce^{3+} phosphor was analysed to study the defect-formation resulting after its irradiation by gamma rays for 30 s. The presence of defects in the material can upset the periodicity of the lattice and disturb the normal band structure, resulting in the formation of localized energy levels within the forbidden gap.[44] TL glow curves were not obtained for $CaZr_4(PO_4)_6$:xDy^{3+} and $CaZr_4(PO_4)_6$:xCe^{3+} phosphors. Consequently, the TL glow curve analysis included here is solely for $CaZr_4(PO_4)_6$:Dy^{3+}, Ce^{3+} phosphor.

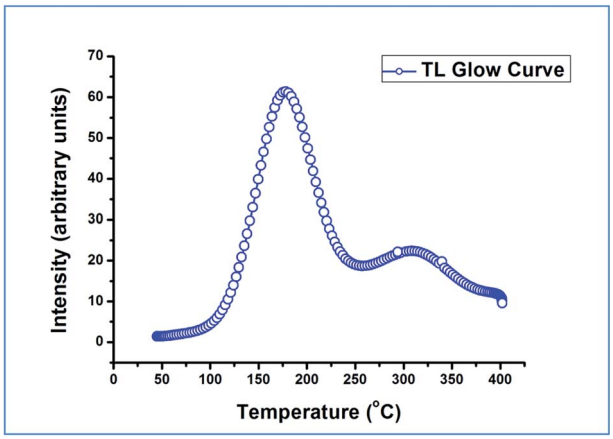

Fig. 21 TL glow curve of γ-irradiated $CaZr_4(PO_4)_6$:0.05Dy^{3+}, 0.05Ce^{3+} phosphor.

Several methods were employed to analyze the TL glow curve and to determine the essential trapping parameters such as activation energy or the trap depth (E), frequency factor (s) and the order of kinetics (b). Fig. 21 represents the TL glow curve of γ-irradiated $CaZr_4(PO_4)_6$:0.05Dy^{3+}, 0.05Ce^{3+} phosphor. Using a linear heating rate (β) of 5 °C s^{-1}, the TL glow curve reveals that the peak temperature at maximum intensity is positioned at 178.24 °C.

3.6.1 Initial rise method. The initial rise method, first suggested by Garlick and Gibson,[45] is based on the analysis of low temperature interval of the peak. This method can be applied to any order of kinetics and the evaluation of the activation energy (E) does not require any knowledge of the frequency factor (s). The initial rise method can be applied only when the glow curve is well defined and clearly separated from other peaks.[46] This method involves plotting a graph of $\ln(I)$ *versus* $1/kT$, for which a straight line is obtained and the negative of the slope of the line gives the activation energy. The activation energy can be calculated by means of the equation,

$$E = -k\frac{\mathrm{d}\,(\ln I)}{\mathrm{d}\left(\frac{1}{T}\right)}$$

where k = Boltzmann's constant.

Table 1 Photometric characteristics of prepared phosphors

Sr. no.	Phosphor	Concentration (mol%)	CIE chromaticity coordinates		Correlated Color temperature (CCT)
			x	y	
(a)	$CaZr_4(PO_4)_6$:xDy^{3+}	$x = 2$	0.3521	0.4101	4957 K
(b)		$x = 3$	0.3676	0.4158	4537 K
(c)		$x = 4$	0.3693	0.4217	4525 K
(d)		$x = 5$	0.3741	0.4261	4437 K
(e)		$x = 6$	0.3707	0.4229	4575 K
(f)	$CaZr_4(PO_4)_6$:xDy^{3+}, yCe^{3+}	$x = 5$, $y = 5$	0.3114	0.3501	6413 K

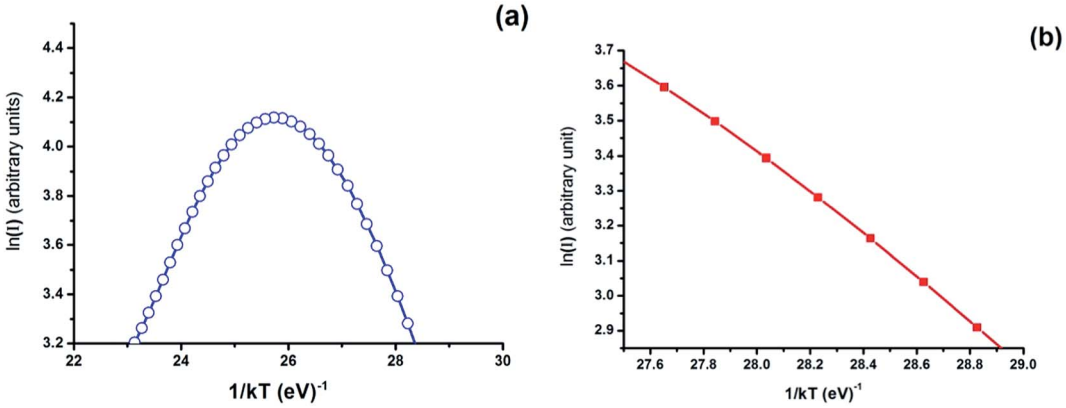

Fig. 22 TL glow curve analysis of $CaZr_4(PO_4)_6$:0.05Dy^{3+}, 0.05Ce^{3+} phosphor by initial rise method.

A regression line through the first 7 data points is shown in Fig. 22(b). The slope of the regression line gives the activation energy $E = 0.5248 \pm 0.012$ eV, with $R^2 = 0.9974$.

3.6.2 Ilich method. Ilich proposed a graphical method as an alternative to the initial rise method.[47] In this method, a cut-off temperature T_c, corresponding to the TL intensity I_c is determined by drawing a tangent to the initial rise of the TL glow peak at the point I_c. The intensity I_c is smaller than about 15% of the maximum TL intensity I_m. The intersection of the tangent to the temperature axis gives the lower temperature T_o. The activation energy is calculated using the formula,

$$E = \frac{kT_c^2}{T_c - T_o}$$

where k = Boltzmann's constant.

From the Fig. 23, the following temperatures were determined:

$$T_c = 115.32\ ^\circ\text{C} = 388.47\ \text{K},\ T_o = 96.90\ ^\circ\text{C} = 370.05\ \text{K}$$

Incorporating these values in the above formula yielded the activation energy $E = 0.7026$ eV.

3.6.3 Analysis based on the shape of the glow curve. The methodology based on analysis of the TL glow peak, by considering the shape or geometrical properties of the peak, established its popularity in discovering the essential parameters E, s and b. Usually, this method requires certain parameters to be pre-defined before proceeding to the actual calculations. For this purpose, a graph is plotted and the following parameters are defined:

T_m is the peak temperature at the maximum.

T_1 and T_2 are, respectively, the temperatures on either side of T_m, corresponding to half intensity.

$\tau = T_m - T_1$ is the half-width at the low temperature side of the peak.

$\delta = T_2 - T_m$ is the half-width toward the fall-off side of the glow peak.

$\omega = T_2 - T_1$ is the total half-width.

$\mu = \delta/\omega$ is the geometrical shape or symmetry factor.

$\rho = \delta/\tau$ is the Balarin's symmetry factor that decides the order of the kinetics.

Using the experimental data, a graph was plotted as shown in Fig. 24 which gave an estimate of the following temperatures:

$$T_m = 178.24\ ^\circ\text{C} = 451.39\ \text{K},\ T_1 = 141.44\ ^\circ\text{C} = 414.59,$$
$$T_2 = 219.68\ ^\circ\text{C} = 492.83\ \text{K}$$

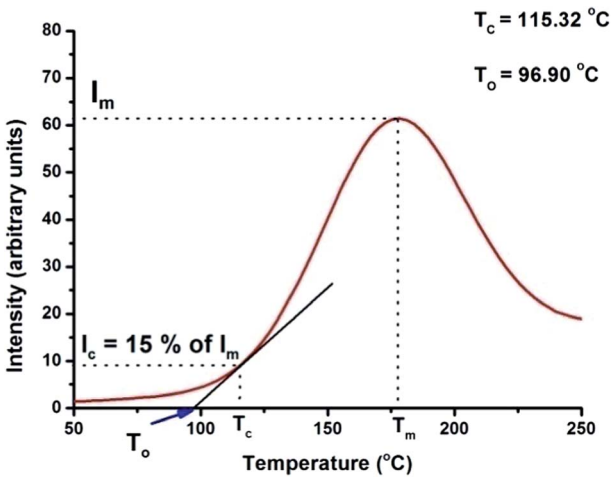

Fig. 23 TL glow curve analysis of $CaZr_4(PO_4)_6$:0.05Dy^{3+}, 0.05Ce^{3+} phosphor by Ilich method.

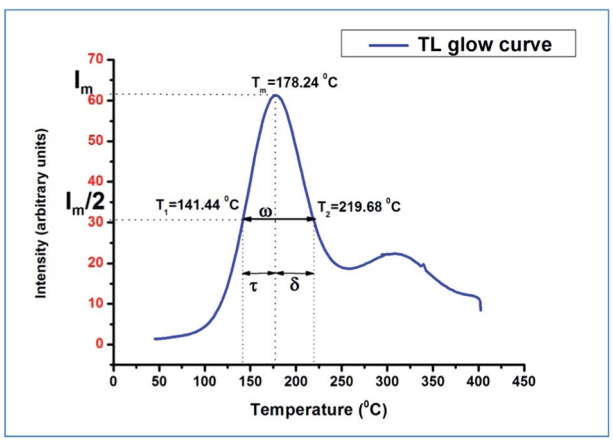

Fig. 24 TL glow curve analysis of $CaZr_4(PO_4)_6$:0.05Dy^{3+}, 0.05Ce^{3+} phosphor by Chen's method.

$$\omega = T_2 - T_1 = 78.24\ \text{K},\ \tau = T_m - T_1 = 36.8\ \text{K},$$
$$\delta = T_2 - T_m = 41.44\ \text{K}$$

The calculated value of the geometrical shape factor $\mu = \delta/\omega = 0.5296$ is in close proximity with the theoretical value for a second order TL peak $\mu = \delta/\omega = 0.52$. This confirms that the TL peak under study shows second order kinetics, which supports the probability of retrapping of the released charge carriers before recombination. The Balarin's symmetry factor, in this case, is calculated to be $\rho = \delta/\tau = 1.126$. With an intention to determine the activation energy, we apply Chen's equation for second-order kinetics.

Using the value of τ:

$$E = \frac{1.81\ k\ {T_m}^2}{\tau} - 2(2kT_m) = 0.8594 - 0.1548 = 0.7046\ \text{eV}$$

Using the value of δ:

$$E = \frac{1.71\ k\ {T_m}^2}{\delta} = 0.7210\ \text{eV}$$

Using the value of ω:

$$E = \frac{3.54\ k\ {T_m}^2}{\omega} - 2kT_m = 0.7906 - 0.0774 = 0.7132\ \text{eV}$$

Several other methods based on the shape of the TL glow peak has been introduced for further verification of the activation energy. One such method used in the present study is the one proposed by Lushihik[48] for second-order kinetics by inducting the parameter δ defined above. Evaluation of the activation energy for second order kinetics can be performed using Lushihik's formula,

$$E = \frac{2\ k\ {T_m}^2}{\delta}$$

The facile calculations of the activation energy using the above formula gives $E = 0.8434$ eV.

Another approach, made by Halperin and Braner, uses an iterative process to find E using both T_1 and T_2 on the glow curve.[49] Execution of their equation,

$$E = \frac{2\ k\ {T_m}^2}{\tau}(1 - 3\Delta_m);\ \text{where}\ \Delta_m = \frac{2\ k\ T_m}{E}$$

resulted in a number of iterations giving the final value of activation energy $E = 0.6715$ eV.

Chen embellished the equations with a new approximation method that overcomes several difficulties and does not include complicated iterative methods. The new approximated equation for second order kinetics is given by,

$$E = 2\ kT_m\left(1.76\ \frac{T_m}{\omega} - 1\right)$$

Using Chen's approximation method, the activation energy was determined as $E = 0.7087$ eV.

Table 2 Trapping parameters of $CaZr_4(PO_4)_6$:0.05Dy^{3+}, 0.05Ce^{3+} phosphor calculated by different methods

Sr. no.	Parameter	Calculated value
1	Activation energy (E)	
	(a) Initial rise method	0.5248 ± 0.012 eV
	(b) Ilich method	0.7026 eV
	(c) Chen's τ-equation	0.7046 eV
	(d) Chen's δ-equation	0.7210 eV
	(e) Chen's ω-equation	0.7132 eV
	(f) Lushihik's formula	0.8434 eV
	(g) Halperin and Braner method	0.6715 eV
	(h) Chen's approximation method	0.7087 eV
2	Order of kinetics (b)	2
3	Frequency factor (s)	$2 \times 10^7\ s^{-1}$
4	Geometrical shape or symmetry factor (μ)	0.5296
5	Balarin's parameter (ρ)	1.126

Once the value of activation energy has been determined, the frequency factor (s) can be easily calculated using the Chen–Winner equation:

$$s = \frac{\beta\ E\ e^{\left(\frac{E}{k\ T_m}\right)}}{k\ {T_m}^2}\left[1 + (b-1)\frac{2kT_m}{E}\right]$$

where β is the heating rate, *i.e.* 5°C s^{-1} and b is the order of the kinetics. In this case $b = 2$.

The calculated values of activation energy using different methods along with the values of other parameters are summarized in the tabular form in Table 2.

All these parameters serve as an aid to understand the defect chemistry responsible for trapping and emission in the material. The TL peak exhibits a second order kinetics with a symmetry factor very close to the standard theoretical value. In this case, the emission of light is delayed by the retrapping of the electrons in the trap and this delay mostly appears during the descending part of the TL glow curve. It might be expected that such curves will show reasonably more thermoluminescence during the second half of the peak in comparison with the first order curve. The TL glow peak intensity of $CaZr_4(PO_4)_6$:0.05Dy^{3+}, 0.05Ce^{3+} phosphor is found to be very less and hence, an inference could be made that negligible amount of defects are produced in the phosphor for 2.6 Gy irradiation of gamma rays.

4. Conclusion

In conclusion, $CaZr_4(PO_4)_6$:Dy^{3+}, $CaZr_4(PO_4)_6$:Ce^{3+} and $CaZr_4(PO_4)_6$:Dy^{3+}, Ce^{3+} phosphors have been synthesized *via* the solid state reaction method. Analysis of the Raman spectrum identified the normal vibrational modes of the PO_4^{3-} tetrahedron. The PL emission spectra of $CaZr_4(PO_4)_6$:Dy^{3+} phosphors, when excited at 351 nm, exhibited two prominent peaks at around 483 nm and 576 nm which are corresponding to $^4F_{9/2} \rightarrow {}^6H_J$ (J = 15/2, 13/2) transitions of Dy^{3+} ion, respectively. Concentration quenching of Dy^{3+} ion emission was observed when the Dy^{3+}

doping level exceeded 5 mol%. As per Dexter's theory, concentration quenching is a consequence of the electric dipole–dipole (d–d) interaction. The emission spectra of $CaZr_4(PO_4)_6$:Ce^{3+} phosphors show broad band emission at 338 nm when excited at 276 nm UV wavelength. The critical concentration for this phosphor is found to be 5 mol% and beyond this limit, concentration quenching occurs due to the energy transfer among the nearest neighbouring ions. It is indicated that the $Ce^{3+} \rightarrow Dy^{3+}$ energy transfer process takes place in the host matrix of $CaZr_4(PO_4)_6$. From the photometric characterization, the color temperature and CIE 1931 chromaticity coordinates of the $CaZr_4(PO_4)_6$:Dy^{3+}, Ce^{3+} phosphor is found to be 6413 K and (0.3127, 0.3290), respectively. Although the spectral power distribution of this phosphor is different from that of the D_{65} illuminant, there is a slight similarity in their color temperatures and CIE chromaticity coordinates. These results suggest that the phosphor may be a potential D_{65} simulator. The thermoluminescence study on the co-doped phosphor suggests its stability to low dose of γ-ray exposure. The trapping parameters of this phosphor have been determined using different analysis methods and it is confirmed that negligible defects are formed in the phosphor for 2.6 Gy dose of γ-ray exposure. Due to the efficient excitation in the near-UV region, $CaZr_4(PO_4)_6$:Dy^{3+}, Ce^{3+} phosphors could be potential candidates for white light emitting diodes (LEDs) fabricated with near-UV chips.

Acknowledgements

The authors are grateful to Dr P. K. Bajpai (Guru Ghasidas University, Bilaspur) for providing access to the Raman Spectroscopy.

References

1 J. Dwivedi, P. Kumar, A. Kumar, Sudama, V. N. Singh, B. P. Singh, S. K. Dhawan, V. Shanker and B. K. Gupta, *RSC Adv.*, 2014, **4**, 54936.
2 C. K. Gana, A. F. Sapara, Y. C. Muna and K. E. Chong, *Procedia Eng.*, 2013, **53**, 208.
3 W. R. Ryckaert, K. A. G. Smet, I. A. A. Roelandts, M. Van Gils and P. Hanselaer, *Energy and Buildings*, 2012, **49**, 429.
4 S. Ye, F. Xiao, Y. X. Pan, Y. Y. Ma and Q. Y. Zhang, *Mater. Sci. Eng., R*, 2010, **71**, 1.
5 M. Shang, C. Li and J. Lin, *Chem. Soc. Rev.*, 2014, **43**, 1372.
6 Z.-W. Zhang, L. Liu, X.-F. Zhang, J.-P. Zhang, W.-G. Zhang and D.-J. Wang, *Spectrochim. Acta, Part A*, 2015, **137**, 1.
7 X. Wu, Y. Liang, R. Chen, M. Liu and Z. Cheng, *Mater. Chem. Phys.*, 2011, **129**, 1058.
8 G. V. L. Reddy, L. R. Moorthy, T. Chengaiah and B. C. Jamalaiah, *Adv. Mater. Lett.*, 2013, **4**, 841.
9 S. L. Dong, H. H. Lin, T. Yu and Q. Y. Zhang, *J. Appl. Phys.*, 2014, **116**, 023517.
10 G. Blasse and B. C. Grabmaier, *Luminescent Materials*, Springer-Verlag Press, Berlin, 1994.
11 J. Sun, Z. Lian, G. Shen and D. Shen, *RSC Adv.*, 2013, **3**, 18395.
12 A. Kumari, A. Pandey, R. Dey and V. K. Rai, *RSC Adv.*, 2014, **4**, 21844.
13 S. S. Kang, J. K. Park, J. Y. Choi, S. H. Nam, M. G. Kwak, S. S. Choi and Y. S. Song, *Jpn. J. Appl. Phys.*, 2004, **43**, L1507.
14 X. Zhaoxian, C. Yayong, C. Zhihui and S. Chunxiao, *J. Rare Earths*, 2006, **24**, 133.
15 P. Li, Z. Wang, Q. Guo and Z. Yang, *RSC Adv.*, 2015, **5**, 4448.
16 J. Cho, B. K. Bang, S. J. Jeong and C. H. Kim, *RSC Adv.*, 2014, **4**, 23218.
17 Q. Wu, Y. Li, X. Wang, Z. Zhao, C. Wang, H. Li, A. Mao and Y. Wang, *RSC Adv.*, 2014, **4**, 39030.
18 C.-H. Huang, Y.-T. Lai, T.-S. Chan, Y.-T. Yeh and W.-R. Liu, *RSC Adv.*, 2014, **4**, 7811.
19 W. Schnick, R. Bettenhausen, B. Götze, H. A. Höppe, H. Huppertz, E. Irran, K. Köllisch, R. Lauterbach, M. Orth, S. Rannabauer, T. Schlieper, B. Schwarze and F. Wester, *Z. Anorg. Allg. Chem.*, 2003, **629**, 902.
20 T. Jüstel, P. Huppertz, D. U. Wiechert and D. Uhlich, Light emitting device with a Eu-comprising phosphor material, World Patent Application no. 2007/080541 2007.
21 N. Chakraborty, D. Basu and W. Fischer, *J. Eur. Ceram. Soc.*, 2005, **25**, 1885.
22 W. Fischer, L. Singheiser, D. Basu and A. Dasgupta, *Powder Diffr.*, 2004, **19**, 153.
23 W. Geng, G. Zhu, Y. Shi and Y. Wang, *J. Lumin.*, 2014, **155**, 205.
24 M. Hirayama, N. Sonoyama, A. Yamada and R. Kanno, *J. Solid State Chem.*, 2009, **182**, 730.
25 K. Momma and F. Izumi, *J. Appl. Crystallogr.*, 2011, **44**, 1272.
26 R. Chourasia and O. P. Shrivastava, *Solid State Sci.*, 2011, **13**, 444.
27 B. K. Grandhe, V. R. Bandi, K. Jang, S.-S. Kim, D.-S. Shin, Y.-I. Lee, J.-M. Lim and T. Song, *J. Alloys Compd.*, 2011, **509**, 7937.
28 J. Garcia Sole, L. E. Bausa and D. Jaque, *An Introduction to the Optical Spectroscopy of Inorganic Solids*, John Wiley and Sons Ltd., West Sussex, 2005.
29 Z. Yang, H. Dong, X. Liang, C. Hou, L. Liu and F. Lu, *Dalton Trans.*, 2014, **43**, 11474.
30 S. Dutta, S. Som and S. K. Sharma, *Dalton Trans.*, 2013, **42**, 9654.
31 *Spectra and Energy Levels of Rare Earth Ions in Crystals*, ed. G. H. Dieke, H. M. Crosswhite and H. Crosswhite, Wiley, New York, 1968.
32 G. Blasse, *J. Solid State Chem.*, 1986, **62**, 207.
33 D. L. Dexter and J. H. Schulman, *J. Chem. Phys.*, 1954, **22**, 1063.
34 D. L. Dexter, *J. Chem. Phys.*, 1951, **21**, 836.
35 C. J. Duan, Z. J. Zhang, S. Rosler, S. Rosler, A. Delsing, J. T. Zhao and H. T. Hintzen, *Chem. Mater.*, 2011, **23**, 1851.
36 R. Yu, S. Zhong, N. Xue, H. Li and H. Ma, *Dalton Trans.*, 2014, **43**, 10969.
37 J. W. H. van Krevel, H. T. Hintzen, R. Metselaar and A. Meijerimk, *J. Alloys Compd.*, 1998, **268**, 272.
38 L. G. Van Uitert, *J. Electrochem. Soc.*, 1967, **114**, 1048.
39 M. Shang, D. Geng, Y. Zhang, G. Li, D. Yang, X. Kang and J. Lin, *J. Mater. Chem.*, 2012, **22**, 19094.

40 Y. M. Lam and J. H. Xin, *Color Res. Appl.*, 2002, **27**, 243.
41 M. Grundmann, *The Physics of Semiconductors*, Springer-Verlag Berlin, 2010.
42 N. Ohta and A. R. Robertson, *CIE Standard Colorimetric System, in Colorimetry: Fundamentals and Applications*, John Wiley & Sons, Ltd, Chichester, UK, 2005.
43 B. P. Kore, N. S. Dhoble, S. P. Lochab and S. J. Dhoble, *RSC Adv.*, 2014, **4**, 49979.
44 B. P. Kore, N. S. Dhoble and S. J. Dhoble, *J. Lumin.*, 2014, **150**, 59.
45 G. F. J. Garlick and A. F. Gibson, *Proc. Phys. Soc.*, 1948, **60**, 574.
46 S. W. S. Mckeever, *Thermoluminescence of Solids*, Cambridge University Press, 1983.
47 B. M. Ilich, *Soviet Physics, Solid State*, 1979, **21**, 1880.
48 L. I. Lushihik, *Soviet physics JETP*, 1956, **3**, 390.
49 A. Halperin and A. A. Braner, *Phys. Rev.*, 1960, **117**, 408.